Mon. Not. R. Astron. Soc. **000**, 1–10 (2007) Printed 2 February 2008 (MN LATEX style file v2.2)

Width of X-ray lines as a diagnostic of gas motions in cooling flows

P. Rebusco [1,5], E. Churazov[1,2], R. Sunyaev[1,2], H. Böhringer[3], W. Forman[4]
[1] *Max-Planck-Institut für Astrophysik, Karl-Schwarzschild-Strasse 1, 85741 Garching, Germany*
[2] *Space Research Institute (IKI), Profsoyuznaya 84/32, Moscow 117810, Russia*
[3] *MPI für Extraterrestrische Physik, P.O. Box 1603, 85740 Garching, Germany*
[4] *Harvard-Smithsonian Center for Astrophysics, 60 Garden St., Cambridge, MA 02138, USA*
[5] *Kavli Institute for Astrophysics and Space Research, MIT, Cambridge, MA 02139, USA*

2 February 2008

ABSTRACT

The dissipation of turbulent gas motions is one of the likely mechanisms that has been proposed to heat the intracluster medium (ICM) in the cores of clusters and groups of galaxies. We consider the impact of gas motions on the width of the most prominent X-ray emission lines. For heavy elements (like iron) the expected linewidth is much larger than the width due to pure thermal broadening and the contribution due to turbulent gas motions should be easily detected with the new generation of X-ray micro-calorimeters, such as the Spektr-RG calorimeter (SXC). For instance in the Perseus cluster the turbulent velocity required to balance radiative cooling (as derived by Rebusco et al. 2006), would imply a width of the 6.7 keV Fe line of 10-20 eV, while the pure thermal broadening is ∼4 eV. The radial dependence of the linewidth is sensitive to i) the radial dependence of the velocity amplitude and ii) the "directionality" of the stochastic motions (e.g. isotropic turbulence or predominantly radial gas motions). If the width of several lines, characteristic for different gas temperatures, can be measured, then it should be possible to probe both the "directionality" and the amplitude of the gas motions. Moreover a measurement of the width would put a lower limit on the amount of the kinetic energy available for dissipation, giving a constraint on the ICM models.

Key words: turbulence - line:profiles - cooling flows - clusters:individual:Perseus

1 INTRODUCTION

Clusters of galaxies are the largest gravitationally bound and nearly virialized systems in the Universe. High resolution X-ray surveys have revealed that the ICM (with temperatures in the range $\sim 2-10$ keV) is not fully relaxed. The substructures in the surface brightness and temperature are observed both on large scales and in the cluster cores indicating that the gas is not at rest. At the same time strong shocks are rarely observed (see Markevitch & Vikhlinin, 2007 for a review) suggesting that the cluster gas motions are predominantly subsonic. The shape of the emission lines as a source of information on the ICM velocity distribution has been discussed in detail in Sunyaev, Norman & Bryan (2003) and Inogamov & Sunyaev (2003). These papers mostly consider the gas motions induced by cluster mergers. In the present paper we focus on the linewidth as a diagnostic of gas motions in the cores of the galaxy clusters.

In the cores of most clusters and many groups (e.g. Stewart et al 1984, Nulsen et al 1984, Edge & Stewart 1991, Mulchaey et al 1993, Fabian 1994), the radiative cooling time of the gas is short compared to the age of the cluster and an external source of energy is needed to avoid catastrophic cooling (e.g. David et al. 2001, Matsushita et al. 2002, Peterson et al. 2003, Kaastra et al. 2004). The dissipation of turbulent gas motions is one of the highly plausible sources of the required energy (e.g. Pedlar et al. 1990, Churazov et al. 2002, Fabian et al. 2003a, Chandran 2005). These motions can have distinctive effects on the properties of the X-ray lines (e.g. Brüggen, Hoeft & Ruszkowski 2005). There are several indirect ways of probing the gas velocities, i) using the resonant scattering of the brightest emission lines (e.g. Gilfanov, Sunyaev & Churazov, 1987, Churazov et al., 2004); ii) considering the spreading of metals ejected by a central galaxy through the ICM (Rebusco et al., 2005,2006, Graham et al., 2006, Roediger et al., 2007); iii) using Hα emitting filaments as tracers of the gas motions (e.g. Fabian et al., 2003b, Hatch et al., 2006). In particular in Rebusco et al. (2005,2006) the characteristic spatial and

velocity scales of the turbulent eddies were estimated assuming that the dissipation of turbulent motions can generate enough heat to prevent the gas from extreme cooling and that the same motions provide moderate mixing of metals through the ICM. Using these constraints we calculated the expected width of the brightest X-ray lines for the brightest clusters (e.g., A426 - Perseus).

A micro-calorimeter with energy resolution of less than 10 eV and effective area of $\sim$ 200 cm^2 has been built for the Suzaku mission (Kelley et al., 2007). The effective areas of the upcoming calorimeters may reach thousands and even tens of thousands of square cm in the next 10-15 years and will have a spatial resolution between a few arcseconds and a few arcminutes (see e.g. `http://www.astro.isas.ac.jp/future/NeXT`, `http://www.rssd.esa.int/index.php?project=XEUS`, `http://constellation.gsfc.nasa.gov/`).

The Spektr-RG Calorimeter (SXC) (McCammon et al., 2007; Mitsuda et al., 2007), proposed for the Spektr-RG Mission, has a peak effective area of 300 cm^2 at $\sim$ 1.5 keV, decreasing to about 30 cm^2 at 6.7 keV and an energy resolution (goal) of $\sim$ 4 eV. As we show in Section 3, an instrument with these characteristics is well suited to study the line broadening associated with turbulent gas motions in the cores of the brightest galaxy clusters.

The structure of the paper is the following. In section 2 we describe the line broadening under different assumptions for the character of the gas motions; in section 3 we consider the specific case of the Perseus cluster as an example and we investigate the capabilities of SXC in this context. Our findings are discussed and summarized in sections 4 and 5.

Throughout the paper when we mention turbulence, we mean all types of macroscopic gas motions.

2 THE IMPACT OF TURBULENCE ON THE LINEWIDTH

There are several bright emission lines in the X-ray range, that are characteristic of the ICM in galaxy clusters (Table 1). The He-like iron line at 6.7 keV is the most prominent feature above a few keV: it is especially bright in high temperature ($T_e > 4$ keV) clusters. For the lower temperature clusters, and in particular for the cooling flow regions, L lines of iron at $\sim$1 keV, lines of Si, Mg and O can be substantially brighter than the 6.7 keV line. In Table 1 we list a sub-sample (incomplete) of these lines and provide an estimate of their fluxes from the central 5′ (radius) region of the Perseus cluster. All line parameters were taken from the ATOMDB data base (Smith et al. 2001a,b).

Let us first assume that i) the cluster is spherically symmetric, ii) the characteristic correlation length of the velocity field is much smaller than the characteristic dimensions of the system and iii) at each location the emission line profile can be approximated by a Gaussian:

$$p(\nu-\nu_0) = \frac{1}{\sqrt{2\pi}}\frac{1}{\sigma_\nu}\exp\left(-\frac{1}{2}\frac{(\nu-\nu_0)^2}{\sigma_\nu^2}\right), \quad (1)$$

where ν_0 is the frequency of the transition and and ν is the observed frequency, $\sigma_\nu = \sigma_\nu(R)$ is the width of the line, which is a function of the distance R from the cluster center. The spectral surface brightness in a line at a given projected distance (x) from the center of the cluster is given by the following integral along the line of sight (l):

$$I(\nu,x) = \int_{-\infty}^{\infty} n_e^2\ a\ \epsilon_{\nu_0}\ p(\nu-\nu_0)\ dl, \quad (2)$$

where $n_e = n_e(R)$ is the electron density, $a = a(R)$ the element abundance, $\epsilon_{\nu_0} = \epsilon_{\nu_0}(T_e(R))$ the plasma emissivity in a given line, which is a function of the plasma temperature $T_e(R)$. In the above expression $R = \sqrt{x^2+l^2}$. The line broadening is decomposed into two components:

$$\sigma_\nu^2 = \sigma_{thermal}^2 + \sigma_{turb}^2, \quad (3)$$

where

$$\sigma_{thermal} = \nu_0\frac{\sqrt{\frac{kT_e}{Am_p}}}{c}$$
$$\sigma_{turb} = \nu_0\frac{v_\parallel}{c}, \quad (4)$$

where k is the Boltzmann constant, m_p the proton mass, A the atomic weight of the element, c the speed of light and $v_\parallel$ the line of sight component of the turbulent velocity. For the case of isotropic turbulence, $v_\parallel^2 = v_{turb}^2/3$, where v_{turb} is the root-mean-square of the 3-dimensional turbulent velocity. A comparison of thermal and turbulent broadenings in a 4 keV plasma is given in Table 2. Note that even for the iron line at 6.7 keV, the natural width of the line due to radiative decay is only $\sim$0.2 eV (and it is much lower for the other transitions in Table 2). We therefore neglect the natural width of all the lines throughout this paper.

It is obvious from equation 4 that the heaviest elements are the best probes of gas motions, since more massive nuclei have smaller thermal line broadening and, therefore, the turbulent broadening can dominate the thermal broaden-

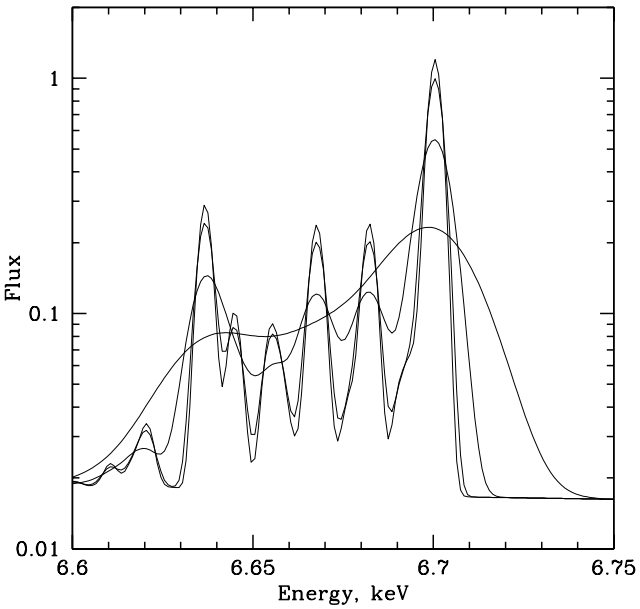

Figure 1. 6.7 keV line complex for a T =4 keV plasma. The four spectra correspond to thermal broadening and turbulent broadening with v_{turb}=0, 100, 300 and 900 km/s. For comparison the sound speed in a 4 keV plasma is $\sim$1000 km/s.

Ion	Z	u	l	E keV	$\epsilon_{\rm peak}$ phot cm^3 s^{-1}	$T_{\rm peak}$ keV	F($<5'$) $\times10^{-3}$ erg cm^{-2} s^{-1}
FeXXV	26	$1s2p\ ^1P_1$	$1s^2\ ^1S_0$	6.700	4.56×10^{-17}	5.42	1.25
FeXXIV	26	$1s^23p\ ^2P_{3/2}$	$1s^22s\ ^2S_{1/2}$	1.1675	9.92×10^{-17}	1.74	2.72
SiXIV	14	$2p\ ^2P_{3/2}$	$1s\ ^2S_{1/2}$	2.006	5.02×10^{-17} [a]	<1.50	1.38
MgXII	12	$2p\ ^2P_{3/2}$	$1s\ ^2S_{1/2}$	1.470	4.26×10^{-17} [a]	<1.50	1.17
OVIII	8	$2p\ ^2P_{3/2}$	$1s\ ^2S_{1/2}$	0.650	2.26×10^{-16} [a]	<1.50	6.21

Table 1. Emission lines: (1) ion, (2) atomic number Z, (3)-(4) respectively, upper and lower levels of the transition, (5) line energy in keV, (6) peak emissivity within the temperature range of interest $1.5-10$ keV, (7) temperature (in the range $1.5-10$ keV) at which the emissivity is the highest for a given line, (8) estimated flux of the line (phot cm^{-2} s^{-1}) for the central $5'$ region of the Perseus cluster. (a) Line emissivity at T =1.5 keV. The true peak emissivity in this line is at a temperature below 1.5 keV.

Ion, E(keV)	v_{turb}(km/s)	FWHM$_{thermal}$(eV)	FWHM$_{turb}$(eV)	$\frac{FWHM_{total}}{FWHM_{thermal}}$
FeXXV, 6.700	100	4.35	3.04	1.22
	300	4.35	9.12	2.30
	900	4.35	27.35	6.31
FeXXIV, 1.170	100	0.76	0.53	1.22
	300	0.76	1.59	2.32
	900	0.76	4.78	6.36
SiXIV, 2.006	100	1.84	0.91	1.12
	300	1.84	2.73	1.79
	900	1.84	8.19	4.55
MgXII, 1.470	100	1.46	0.67	1.10
	300	1.46	2.00	1.70
	900	1.46	6.00	4.23
OVIII, 0.650	100	0.79	0.29	1.07
	300	0.79	0.88	1.50
	900	0.79	2.65	3.50

Table 2. Thermal and turbulent broadening in a 4 keV plasma: (1) line energy in keV, (2) turbulent velocity in km/s, (3) FWHM due to pure thermal broadening, (4) FWHM due to isotropic turbulent broadening alone, (5) ratio of the total FWHM to pure thermal broadening.

ing. Indeed the ratio of the e.g. iron thermal velocity to the proton thermal velocity is small ($\sim (m_p/Am_p)^{1/2} = 0.13$). Thus even for small velocities the turbulent broadening will exceed the thermal broadening (Table 2, Figure 1). For an instrument with a given spectral resolution the energy of the line also plays an important role, since the width of the line simply scales with the line energy. This makes the iron 6.7 keV line the best probe of the turbulent ICM, as long as the instrument has a substantial effective area at 6-7 keV.

The above assumption of a Gaussian line shape due to turbulent motions is of course only an approximation (see Inogamov & Sunyaev 2003 for a discussion). However it is fully sufficient to assess the detectability of the turbulent broadening. In fully developed turbulence an entire range of scales is produced through an energy cascade (e.g. Richardson 1922, Tennekes & Lumley 1972, Lesieur 1997, Mathieu 2000, Davidson 2004), which is characterized by large scale energy-containing motions and a small dissipation scale. In our simplified treatment we assume that the v_{turb} entering all our equations can be obtained from the kinetic energy of the turbulent motions: $\epsilon_K = \rho\frac{v_{turb}^2}{2}$, where ρ is the gas density. Since the integration of equation 2 may result in a line shape different from a pure Gaussian we use below an "effective" full width half maximum (eFWHM), which is defined as the interval of energies centered at the line energy and containing 76% of the line flux.

2.1 Isotropic, radial and tangential motions

There is indirect evidence that the gas in cluster centers is involved in some sort of motion. Hα emitting filaments, that are thought to be drawn behind buoyant gas bubbles, have been used to trace the ICM velocity field (e.g. Hatch et al. 2006, 2007, Salomé et al. 2007). However neither the characteristic velocity scales nor the characteristic patterns of the hot gas motions have been measured in a more direct way so far. One can identify two major sources of turbulent gas motions in the cores: cluster mergers and the action of a central active galactic nucleus (AGN). Each process may produce a velocity field different in intensity and directionality. Let us consider the extreme cases of isotropic, pure radial and pure tangential velocity fields as illustrated in Figure 2. If one fixes the total kinetic energy in the motions, then the line of sight component of the velocity can be written as:

$$v_\parallel^2 = \begin{cases} \frac{v_{turb}^2}{3} & \text{isotropic,} \\ v_{turb}^2\frac{l^2}{R^2} & \text{radial,} \\ \frac{v_{turb}^2}{2}\frac{x^2}{R^2} & \text{tangential.} \end{cases} \quad (5)$$

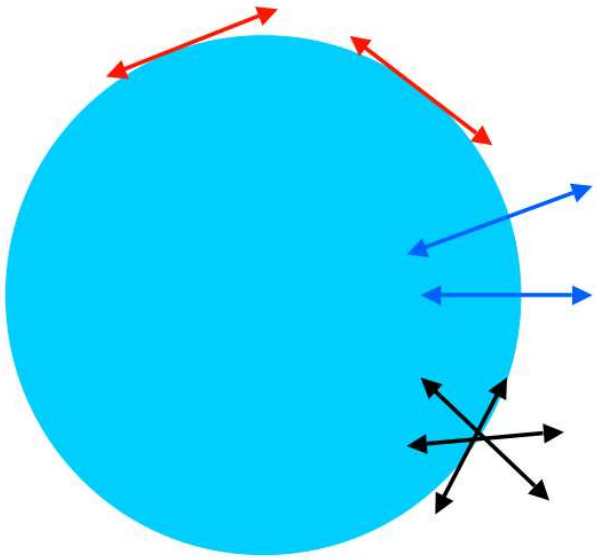

Figure 2. Sketch of isotropic (lower right, black arrows), radial (right, blue arrows) and tangential motions (top, red arrows).

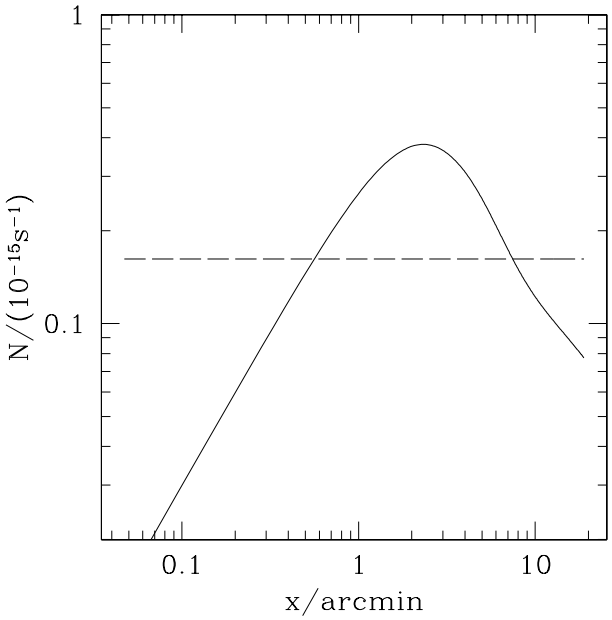

Figure 3. Brunt-Väisälä frequency N (solid line) for the Perseus cluster in comparison with the characteristic frequency of turbulent motions v_{turb}/l for $v_{turb} = 100$ km s^{-1} and $l = 20$ kpc (dashed line). If gravity waves are excited, then they are trapped in the region where the turbulent frequency is smaller than the Brunt-Väisälä frequency.

The first case (isotropic gas motions) can occur for a wide variety of driving mechanisms, ranging from mergers to the motions caused by rising buoyant bubbles of relativistic plasma or to convection driven by a mixture of thermal plasma and cosmic rays (Chandran 2005). Pure radial gas motions would naturally appear if energy generated by a central AGN goes into weak shocks and sound waves (e.g. Fabian et al. 2003, Forman et al. 2005, 2006, Fabian et al. 2006) which propagate through the ICM almost radially from the central source.

The case of pure tangential motions seems to be less natural and it is included mostly for completeness. We note however that in the stratified atmosphere of clusters the characteristic frequencies of the turbulent motions can be smaller than the Brunt-Väisälä frequency:

$$N^2 = g\left(\frac{1}{\gamma}\frac{dP}{dr} - \frac{1}{\rho}\frac{d\rho}{dr}\right), \qquad (6)$$

where g is the gravitational acceleration due to the dark matter potential, ρ is the gas density, P is its pressure and $\gamma = 5/3$ is the adiabatic index. In Figure 3 we plot the Brunt-Väisälä frequency, evaluated for the Perseus cluster, and compare it with the characteristic frequency of turbulent motions v_{turb}/l for $v_{turb} = 100$ km s^{-1} and $l = 20$ kpc. In the range where the turbulent frequency is smaller than the local Brunt-Väisälä frequency, the gas motions may excite gravity waves (e.g. Churazov et al., 2001, 2002, Omma et al., 2004). These waves can propagate and transport energy from a localized patch of turbulent ICM within this region (e.g. in the case of Perseus within a radius of ~ 10 arcmin). Such a process is well known in atmospheric science and oceanography and it may lead to the formation of non-propagating pancake-shaped vortices (e.g. Riley & Lelong 2000). Therefore, one can imagine that patches of predominantly 2-dimensional (tangential) vortices can be created with this mechanism.

We now calculate (Figure 4) the expected width of the iron 6.7 keV line for each of the three limiting cases given in equation 5, for a model cluster with the density parameterized by a simple β model: $n_e = n_e(0)\left[1 + (r/r_c)^2\right]^{-3/2\beta}$, where r_c is the core radius of the cluster and $\beta = 0.3, 0.5, 0.9$. The gas temperature and the abundance of iron are assumed to be constant. The velocity v_{turb} is fixed to 300 km s^{-1}. The thermal broadening (first term in equation 3) is omitted in the calculation of the linewidth, but the level of thermal broadening for a 6 keV plasma is shown for comparison (dashed line). The three plots in Figure 4 correspond to $\beta = 0.3, 0.5, 0.9$ from left to right, respectively. As expected from equation 5, isotropic turbulence produces a linewidth independent of the projected distance from the cluster center. Pure radial gas motions would result in a line whose width is peaked towards the center of the cluster, while pure tangential motions produce the broadest line outside the cluster core. For $x \gg r_c$, the curve approaches asymptotic values (different for each velocity pattern), that are functions of β only. For large β the cluster is more "compact" and the gradients of the width of the line with radius become stronger, while for low β the change of the linewidth is more gradual.

2.2 Radially dependent velocity amplitude

It is quite plausible that the characteristic turbulent velocity scale varies with the distance from the cluster center. If gas motions are driven by the outflows of a central AGN, then their amplitude will likely decrease for large radii, since the energy would be spread over larger masses of gas and it would be partly dissipated at smaller radii. For example, the characteristic amplitude of spherical sound waves

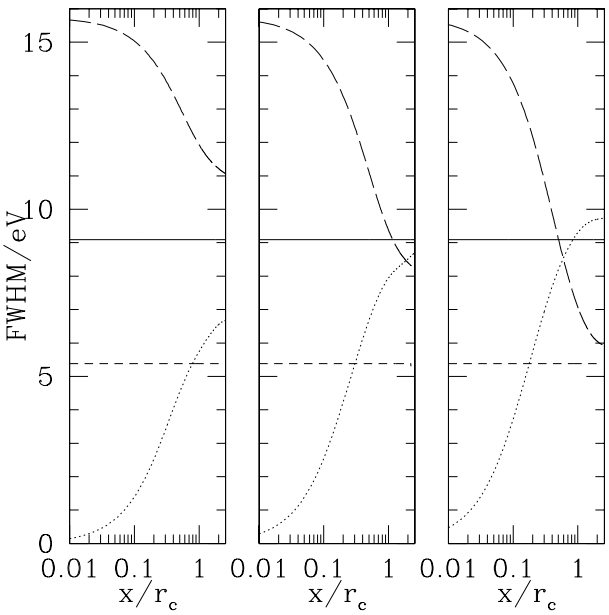

Figure 4. 6.7 keV linewidth as a function of the projected radius, for isotropic (solid), tangential (dotted) and radial (long-dashed) turbulence. The profile is obtained by integrating equation 2, as explained in section 2. In the three panels the gas density profile is different: from left to right $\beta = 0.3, 0.5, 0.9$. The thermal broadening is neglected, but its magnitude in a plasma at 6 keV is shown for reference (short-dashed line).

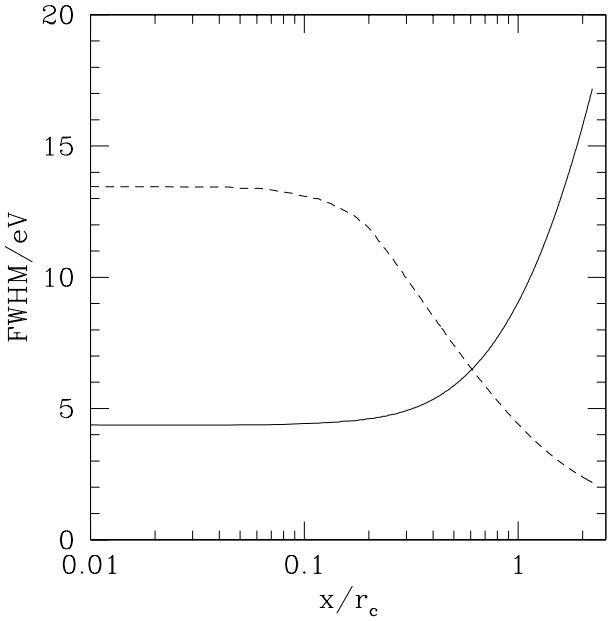

Figure 5. 6.7 keV linewidth as a function of the projected radius, for isotropic turbulence when the velocity scale follows the law $v(R) = v_0 \left(\frac{R}{r_c}\right)^{\alpha}$, with $\alpha = \pm 1$. In each case the velocity scale was assumed to saturate at 1000 km/s. The solid line is for turbulent velocity increasing with radius, the dashed line for turbulent velocity declining with radius. For clarity the thermal broadening is neglected.

propagating through a declining density profile decreases as $v \propto \left(\rho\, R^2\right)^{-1/2}$. For $\rho(R) \propto 1/R$ the velocity varies as $v \propto (R)^{-1/2}$. If, furthermore, dissipation is taking place then the amplitude will decline more quickly, as suggested by Fabian et al. (2003) and studied in three-dimensional viscous simulations by Ruszkowski et al. (2004). For rising buoyant bubbles of relativistic plasma the terminal velocity scales as $v \propto v_K \sqrt{r_b/R}$ (e.g. Churazov et al., 2001), where v_K is the Keplerian velocity at radius R and r_b is the characteristic size of the bubble. The adiabatic expansion of the bubble leads to a slow change of the bubble size $r_b \propto P^{-1/4}$ (assuming that the adiabatic index of the medium inside the bubble is 4/3). Thus the characteristic bubble velocity is $v \propto v_K R^{-1/2} P^{-1/8}$ - a decreasing function of the radius for plausible $v_K(R)$ and $P(R)$. If the bubble breaks down into smaller bubbles, then the terminal velocity will decrease even further with the radius.

Alternatively, if the turbulence is driven by shocks originating from minor mergers, then it is possible that the velocity amplitude will instead decline towards the center, where the gas density and the thermal gas pressure are the highest. For example, for a plane sound wave propagating into a region of increasing density the characteristic velocity is $v \propto \rho^{-1/2}$, i.e. $v \propto R^{1/2}$ if $\rho \propto 1/R$. Here we have ignored both the possible reflection of the sound waves by a steep density gradient (important for long wavelength perturbation) and the focusing of sound waves due to decreasing sound speed towards the center (Pringle, 1989). In reality the effect of mergers on the cluster core is much more complicated and the above estimate can at best be considered as indicative.

For illustration we model two possibilities (decreasing or increasing turbulence) by considering $v(R) = v_0 \left(\frac{R}{r_c}\right)^{\alpha}$, with $\alpha = \pm 1$ and $v_0 = 200$ km/s. We further assume that when $v(R) > 1000$ km/s, the velocity saturates at 1000 km/s. The resulting linewidth profiles are shown in Figure 5. Clearly the radial dependence of the velocity amplitude can strongly affect the behavior of the linewidth as a function of projected distance.

3 AN EXAMPLE: THE PERSEUS CLUSTER

We now calculate the expected width of the 6.7 keV line by using the Perseus cluster as an example. Perseus (A 426) is the brightest nearby X-ray cluster and it is one of the best-studied cool core clusters, together with M87 and Centaurus. It hosts in its core a luminous elliptical galaxy NGC 1275, containing a bright radio source (3C 84). In the core region a complex substructure is seen in X-ray temperature, X-ray surface brightness and optical light distributions. Such substructure includes holes in the X-ray images due to bubbles of relativistic plasma (Böhringer et al., 1993, Fabian et al. 2000), quasi-spherical ripples (Fabian et al. 2003a) and optical Hα filaments (Fabian et al. 2003b, Hatch et al. 2005).

In our estimates of the expected linewidth in Perseus, we assume that the gas cooling losses are compensated by the dissipation of the turbulent motions at all radii. This is of course a strong and not fully justified assumption, but it provides clear predictions if the turbulent heating is indeed

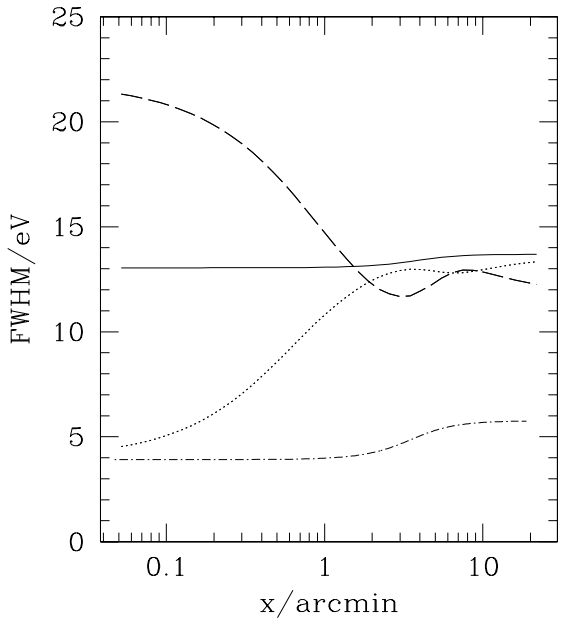

Figure 6. 6.7 keV linewidth as a function of the projected radius in the Perseus cluster for isotropic (solid), radial (long-dashed) and tangential (dotted) motions. The characteristic turbulent velocity $v_{turb} = 410$ km/s was assumed to be constant with radius. The thermal broadening (shown with the short-dashed line) was included in the calculation of the linewidth.

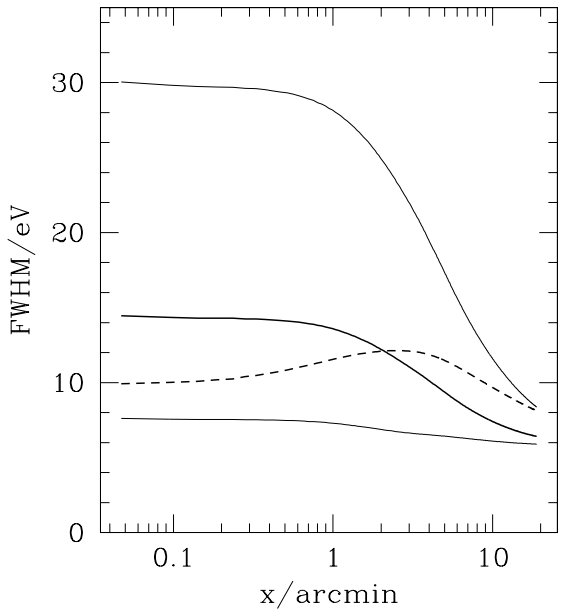

Figure 7. Expected radial dependence of the 6.7 keV linewidth in the Perseus cluster for several illustrative cases. For all curves we assume a balance between gas cooling losses and turbulent heating at each radius according to eq.7. The solid lines correspond to l = 2, 20, 200 kpc (from the bottom to the top respectively), independently of the radius. The dashed line corresponds to the $l = 0.3R$.

important in cluster cores. Thus one can write:

$$C\ \rho\ v_{turb}^3/l \approx n_e^2 \Lambda(T), \quad (7)$$

where $\Lambda(T)$ is the gas cooling function and C is a dimensionless constant of the order of unity (see e.g. Dennis & Chandran, 2005), which depends on the character of the turbulent motions. Since the electron density and temperature are known from observations (e.g. Churazov et al., 2003) one can estimate v_{turb}^3/l from equation 7. As the linewidth depends explicitly on v_{turb} one has to determine (or assume) some constraints on l. For instance, Rebusco et al. (2005, 2006) and Graham et al. (2006) considered the turbulent spreading through the ICM of metals produced by the brightest cluster galaxy. Treating this process in a diffusion approximation one can estimate the effective diffusion coefficient D. In the Perseus cluster $D \sim 2 \times 10^{29}$ cm^2/s (Rebusco et al. 2006). One can then cast D in the form $D = C'\ v_{turb}\ l$, where C' is a dimensionless constant of the order of unity (see Dennis & Chandran 2005 for a compilation of values of C and C'). Combining equation 7 (at some radius) and the expression for the diffusion coefficient, both v_{turb} and l can be measured. In Perseus the characteristic values were found to be $l \sim 20$ kpc and $v_{turb} \sim 410$ km/s (Rebusco et al. 2006). If we adopt v_{turb} =410 km/s as the characteristic velocity of turbulent motions at every radius in Perseus then, depending on the directionality of the turbulence (see Figure 6), the expected width of the 6.7 keV line in Perseus should be in the range 10-20 eV. Of course the above values of l and v_{turb} are only order of magnitude estimates. From equation 7 it is clear that $v_{turb} \propto (n_e\ l\ \Lambda(T))^{1/3}$. If l = const then $v_{turb} \propto n_e^{1/3} \propto R^{-1/3}$ (when $n_e \propto 1/R$). In Figure 7 we calculate the linewidth for several illustrative cases: three solid lines with different thickness correspond to l =2, 20, 200 kpc (at all radii). This spread of two orders of magnitude in l results in a factor of 3 change of the linewidth. If instead we follow the arguments of Dennis & Chandran (2005) and set $l \sim \alpha R$, where $\alpha = 0.3$, then $v_{turb} \approx$ const when $n_e \propto 1/R$. The corresponding curve is shown in Figure 7 by the dashed line.

In order to make some estimates we consider the proposed SXC with an effective area which can be provided by the current generation of X-ray mirrors with a rather short focal length of less than 2 meters. At 6.7 keV the effective area is ~ 30 cm^2. We adopt a spectral and spatial resolution of 4 eV and 1 arcmin respectively. The design goal for SXC is 4 eV resolution, a field of view of 11×11 arcmin square and pixels of 1.8 arcmin square. We want to check how accurately a micro-calorimeter with such parameters will measure the turbulent broadening in the Perseus cluster. The expected number of photon counts in the iron complex in a 1 Msec observation is plotted in Figure 8. Note that, although we focus on the line broadening of the 6.7 keV line, in what follows we use all the photon counts in the 0.5-8.0 keV band, in order to obtain better fits (for reference the number of counts due to the 6.7 keV line accounts for $\sim 0.48\%$ of the total number of counts in the 0.5-8.0 keV band). We simulated the observed spectra using XSPEC, specifically the *bapec* model, which takes into account isotropic broadening. For $v_{turb}^{iso} = 410$ km/s, the component of the velocity along the line of sight is about 237 km/s. An example of the simulated spectrum (for a 1 Msec long observation) is shown in Figure 9. The uncertainty in the measured 6.7 keV line

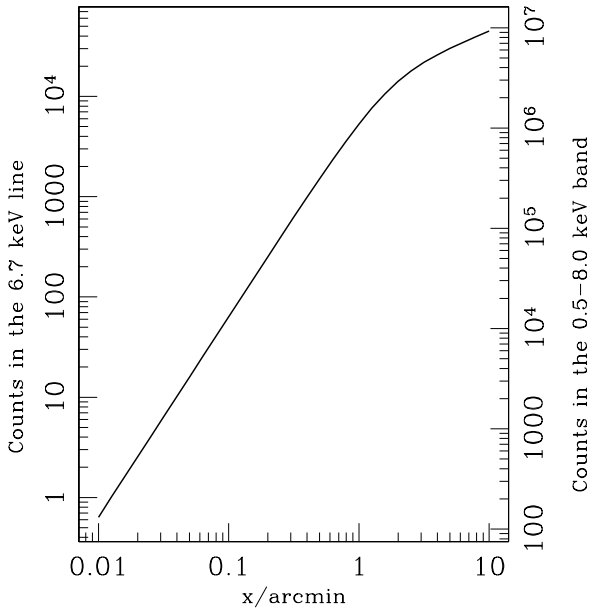

Figure 8. The estimated total photon counts in the 6.7 keV line coming from a circle enclosed in a given projected radius from the Perseus cluster. The assumed duration of the observation is 1 Msec. The counts in the 0.5-8.0 keV band are shown for reference on the right axis.

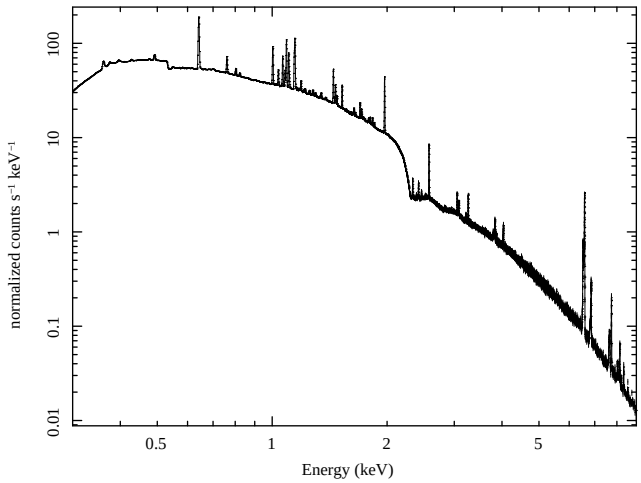

Figure 9. Simulated spectrum of the Perseus cluster core within a radius of $6'$, using the properties of the proposed SXC. The spectrum is derived for $v_{\|} = 236.714$ km/s, $T = 4$ keV and an exposure time of 10^6 s.

broadening as a function of the number of counts is plotted in Figure 10. The solid line shows the true broadening (237 km/s), while the long-dashed and dotted lines indicate the level of 1 sigma confidence for the fitted velocity. The comparison with Figure 8 suggests that already within 0.5 arcmin there are enough photons to measure the turbulent velocity with an uncertainty of $\sim \pm 5$ km/s. Figure 10 assumes a plasma temperature of 4 keV. We repeated the simulations also for higher temperatures and assuming a 2-temperature plasma. In both cases, the turbulent velocity can be recovered with an uncertainty below 15 km/s. In order to test the capabilities of our fiducial micro-calorimeter, we also calculated the accuracy of the fits within each single square of 1.8×1.8 arcmin. Even in the outer parts, the resolution is high enough to measure the turbulent velocity with 1 sigma confidence below 10 km/s. Therefore the spatial dependence of the turbulent velocity could be directly measured and this would give clear indications about the origin of the turbulent gas motions (see Section 2).

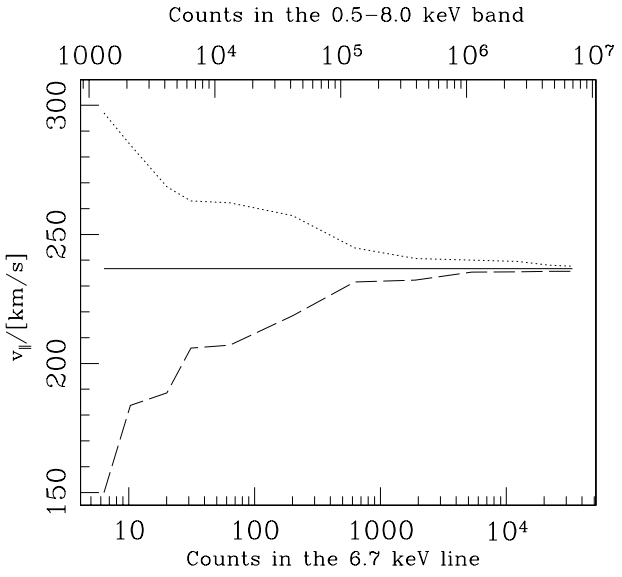

Figure 10. Uncertainty in the measured 6.7 keV line broadening as a function of the number of counts (in the line and in the 0.5-8.0 keV band). The solid line shows the true broadening (237 km/s), while the long-dashed and dotted lines indicate the level of 1 sigma confidence for the fitted velocity. The comparison with Figure 8 suggests that for a circular region with a radius of $0.5'$ in the core of Perseus, the turbulent velocity broadening can be recovered with an uncertainty of about 5 km/s (for a 1 Msec long observation).

4 LINEWIDTH VERSUS SHIFT OF THE LINE CENTROID

All the results obtained in the previous sections are based on the assumption that the characteristic size of the turbulent eddies l is much smaller than the characteristic length of the line of sight.

In practice there are at least two complementary ways of deriving information on the turbulent gas motions with micro-calorimeters. One can use i) the variations of the line centroid with position and/or ii) the width/shape of the line. Assuming that the resolution of the instrument is substantially better than the width of the observed line (e.g. see Fig. 7) the accuracy of determination of the line characteristics (in the case of a strong single line with negligible continuum,

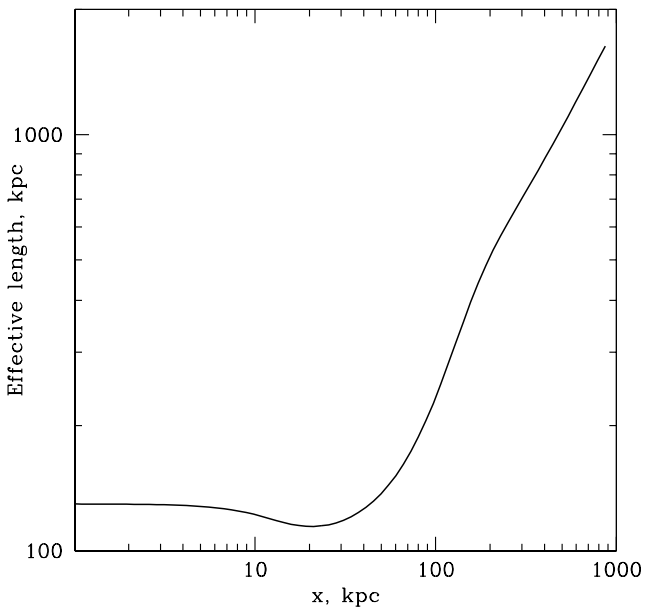

Figure 11. Effective length of the region along the line of sight which provides 75% of the total surface brightness in the 6.7 keV line at a given projected distance from the center of the Perseus cluster. The "dip" around 20-30 kpc is due to the complicated structure in the assumed radial abundance profile (e.g. Schmidt et al. 2002, Churazov et al. 2003).

which corresponds to the most optimistic scenario) is:

$$\sigma_{centroid} \approx \frac{\mathrm{FWHM}_{line}}{2\sqrt{2\ \ln 2}\ \sqrt{N_{counts}}} \quad (8)$$

$$\sigma_{FWHM} \approx \frac{\mathrm{FWHM}_{line}}{\sqrt{2}\ \sqrt{N_{counts}}}, \quad (9)$$

where FWHM_{line} is the width of the line, N_{counts} is the number of counts in the line, $\sigma_{centroid}$ and σ_{FWHM} are the 1σ errors in the centroid and width of the line.

The centroid variation method works best only if the characteristic size of the eddies is not too small. Indeed, in practice one observes the spectrum coming from a selected region of the cluster with characteristic sizes X (in projection) and L (along the line of sight). If $X \gg l$ and $L \gg l$ then $N_{eddies} \sim X^2 L/l^3$ independent eddies are seen by the instrument at the same time. Assuming that each eddy produces a centroid shift of the order of $v_\parallel$, then the observed centroid shift will be $\sim v_\parallel/\sqrt{N_{eddies}} \propto X^{-1}L^{-1/2}$. Increasing X would increase the number of line photons the instrument detects during observations, but this would simultaneously decrease the amplitude of the centroid shift. Obviously these two effects cancel each other and increasing X beyond the characteristic eddy size l does not improve the detectability of the centroid variations. Making X smaller than l would just make the number of line photons smaller: the amplitude of the centroid variation should not vary much. Of course studying the centroid variations on spatial scales larger and smaller than l will be a very useful test of the distribution of characteristic eddy sizes, but for the principal detection of the gas turbulent motions, the choice of $X \approx l$ is obviously the optimal one. Thus the question of prime importance is whether the instrument has an effective area large enough to collect photons from a region with size $X \sim l$ (e.g. sufficient to detect the centroid variations). Of course, averaging along the line of sight remains an unavoidable effect independent of the choice of the region size. In Figure 11 we plot the effective length L of the region along the line of sight which provides 75% of the total surface brightness in the 6.7 keV line, at a given projected distance from the center of the Perseus cluster. It is clear from this figure that, in the core of the Perseus cluster, L is of the order of 130 kpc and it increases linearly outside the core. The non-monotonic behavior of the curve at 20-30 kpc from the center is caused by the complicated iron abundance profile (see e.g. Schmidt et al. 2002, Churazov et al. 2003). Thus, for the optimal size of the observed region, the typical amplitude of the centroid variations will be $v_\parallel/\sqrt{L/l}$. For estimating the centroid variations, we adopt $v_{turb} \sim 400$ km/s (i.e. in the isotropic case $v_\parallel \sim 237$ km/s) and $l \sim 20$ kpc (Rebusco et al., 2006). In the Perseus cluster a single $1.8' \times 1.8'$ SXC pixel, corresponds to a 41×41 kpc region pixel, and an effective length along the line of sight of ~ 100 kpc (see Fig.11). Thus one can expect $\approx 41 * 41 * 100/20^3 = 21$ eddies (assuming a 20^3 kpc^3 volume per eddy) and the typical centroid variations on these spatial scales are of the order of 50 km/s. Such a shift in velocity corresponds to a $\sigma_{line} \sim 1.1$ eV shift in the line energy from pixel to pixel for the 6.7 keV line. From eq. 8 it follows that such variations should be detectable with $\sim 1\sigma$ significance in SXC pixels with ~ 100 counts (for the 6.7 keV line with FWHM of 13 eV - as in Fig. 6). As one can see in Fig. 8 the number of photons in the central pixel for a 1 Msec observation of the Perseus cluster is much higher (of the order of 10^4): hence the centroid variation can be measured with great accuracy.

The detection of the line broadening has no limitation from the point of view of the region size and the whole cooling flow region can be probed at once. According to eq. 9 the 1σ error on the width of the line is ~ 0.3 eV (for the 6.7 keV line with FWHM of 13 eV and number of detected photons $N_{counts} = 1000$). This corresponds to a change in the characteristic velocity scale of ~ 13 km/s. In a 1 Msec observation such broadening can be measured in each of the $1.8' \times 1.8'$ pixels of SXC up to a distance of ~ 5.4 arcminutes from the cluster center (note that SXC's field of view is $\sim 11 \times 11$ arcmin).

From Fig. 10 and from eq. 9 it follows that during a single 1 Msec observation of the Perseus cluster with SXC, the turbulent broadening at the level of a few hundred km/s can be measured in a central $1.8' \times 1.8'$ pixel and a map of the linewidth with the accuracy of the order of 10 km/s covering the area $\sim 11' \times 11'$ can be obtained. Given the expected dependencies of the line broadening shown in Fig.6 and 7, such a dataset would allow one to firmly establish the level of microturbulence in the Perseus cluster and test the hypothesis that turbulent dissipation acts as a mechanism for heating the ICM.

5 CONCLUSIONS

The dissipation of turbulent gas motions driven by AGN activity is a plausible source of heat for the cooling gas in

cluster cores. In this case, we show that the expected width of the iron 6.7 keV line is well above the thermal broadening for most plausible values of the turbulent velocity. In our fiducial model of the Perseus cluster, the 6.7 keV linewidth is larger than 10 eV. Hence the proposed SXC micro-calorimeter is well suited for firmly establishing the level of microturbulence in the brightest galaxy clusters.
As discussed in Sections 2.1 and 2.2 the linewidth is sensitive to both the radial dependence of the velocity amplitude and the "directionality" of the stochastic motions. This may complicate an unambiguous determination of the properties of the gas motions. However this degeneracy can be removed if the width of several lines, characteristic for different gas temperatures, can be measured. Assume for example that in addition to the 6.7 keV iron line, the width of the iron L-shell line is detected. This line is bright at lower temperatures, that are present only in the central region (cool core). Therefore the combined measurement of the width of two or more lines should be sufficient to discriminate among the simplest models with different "directionalities".

ACKNOWLEDGMENTS

We acknowledge the support by the DFG grants CH389/3-2. We would like to thank Dan McCammon, Jan-Willem den Herder, Richard Kelley and Kazu Mitsuda for the data and discussions about SXC. We wish to thank the anonimous referee for his/her useful comments. P.R. is grateful to the International Max Planck Research School for its support, to Andreas Bauswein, Marcus Brüggen and Rasmus Voss for the helpful discussions and to the "Velisti per Caso" of the Adriatica for their enthusiasm.

REFERENCES

Böhringer H., Voges W., Fabian A.C., Edge A.C., Neumann D.M. 1993, MNRAS, 264, L25
Brüggen M., Hoeft M., Ruszkowski M. 2005, ApJ, 628, 153
Chandran B.D.G. 2005, ApJ, 632, 809
Churazov E., Brüggen M., Kaiser C.R., Böringer H., Forman W. 2001, ApJ, 554, 261
Churazov E., Sunyaev R.A., Forman W., Böringer H. 2002, MNRAS, 332, 729
Churazov E.,Forman W., Jones C., Böringer H. 2003, ApJ, 590, 225
Churazov E.,Forman W., Jones C., Sunyaev R., Böringer H. 2004, MNRAS,347, 29
David L., Nulsen P., McNamara B., Forman W., Jones C., Ponman T., Robertson N., Wise M. 2001, ApJ, 557, 546
Davidson P.A. 2004, *Turbulence*, Oxford Univ. Press (New York)
Dennis T., Chandran B. 2005, ApJ, 622, 205
Edge A.C., Stewart G.C. 1991, MNRAS, 252, 414
Fabian A.C. 1994, ARA&A, 32, 277
Fabian A. C. et al., 2000, MNRAS, 318, L65
Fabian A. C., Sanders J.S., Allen S.W., Crawford C.S., Iwasawa K., Johnstone R.M., Schmidt R.W. 2003a, MNRAS, 344, L43
Fabian A.C. et al. 2003b, MNRAS, 344, L48
Fabian A.C., Sanders J.S., Taylor G.B., Allen S.W., Crawford C.S., Johnstone R.M., Iwasawa K. 2006, MNRAS, 366, 417
Forman W. et al. 2005, ApJ, 635, 894
Forman W. et al. 2006, astro-ph/0604583
Gilfanov M.R., Sunyaev R.A., Churazov E. 1987, SvAL, 13, 233
Graham J., Fabian A. C., Sanders J. S., Morris R. G., 2006, MNRAS, 368, 1369
Hatch N.A., Crawford C.S., Fabian A.C. 2007, MNRAS, 380, 33
Hatch N.A., Crawford C.S., Johnstone R.M., Fabian A.C. 2006, MNRAS, 367, 433
Inogamov N.A., Sunyaev R.A. 2003, Astron. Lett., 29,12
Kaastra J.S. et al. 2004,A&A, 413, 415
Lesieur M. 1997, *Turbulence in Fluids*, Reidel Ed. (Dordrecht)
Kelley R. L., et al., 2007, PASJ, 59, 77
Markevitch M., Vikhlinin A. 2007
Mathieu J. 2000, *An introduction to turbulent flow*, Cambridge Univ. Press (Cambridge)
Matsumoto H., Koyama K., Awaki H., Tomida H., Tsuru T., Mushotzky R., Hatsukade I., 1996, PASJ, 48, 201
Matsushita K., Belsole E., Finoguenov A., Böhringer H. 2002, A&A, 386, 77
McCammon D. et al 2007, in preparation
Mitsuda K., Kelley R., McCammon D., den Herder J-W, Ohashi T. 2007, Journal of Low Temperature Physics, in preparation
Mulchaey J.S., Davis D.S., Mushotzky R.F., Burstein D. 1993, ApJ, 404, L9
Nulsen P.E.J., Stewart G.C., Fabian A.C. 1984, MNRAS, 208, 185
Omma H., Binney J., Bryan G., Slyz A. 2004, MNRAS, 348, 1105
Pedlar A. et al. 1990, MNRAS, 246, 477
Peterson J.R., Kahn S.M., Paerels F.B.S., Kaastra J.S., Tamura T., Bleeker J.A.M., Ferrigno C., Jernigan J.G. 2003, ApJ, 590, 207
Pringle J.E. 1989, MNRAS, 239, 479
Rebusco P., Churazov E., Böhringer H., Forman W., 2005, MNRAS, 359, 1041
Rebusco P., Churazov E., Böhringer H., Forman W., 2006, MNRAS, 372, 1840
Richardson, L.F. 1922, Weather Prediction by Numerical Processes, Cambridge Univ. Press
Riley J.J., Lelong M. 2000, Annu.Rev.Fluid Mech., 32, 613
Roediger E., Brüggen M., Rebusco P., Böhringer H., Churazov E. 2007, MNRAS, 375, 15
Ruszkowski M., Brüggen M., Begelman M. C. 2004, ApJ, 615, 675
Salomé P. et al. 2006, A& A 454, 437
Schmidt R.W., Fabian A.C., Sanders J.S. 2002, MNRAS, 337, 71
Smith R.K., Brickhouse N.S., Liedahl D.A., Raymond J.C. 2001a, ApJ, 556, L91
Smith R.K., Brickhouse N.S., Liedahl D.A., Raymond J.C. 2001b, Spectroscopic Challenges of Photoionized Plasmas, ASP Conference Series Vol. 247, 159. Ed. G.Ferland&D. Wolf Savin
Stewart G.C., Fabian A.C., Jones C., Forman W. 1984, ApJ, 285, 1

Sunyaev R.A., Norman M.L., Bryan G.L. 2003, AstL, 29, 783
Tennekes H., Lumley J.L. 1972, *A first course in turbulence*, MIT Press (Cambridge)